

# Giant macro-spicule as observed by CDS on SOHO

D. Banerjee<sup>1,\*</sup>, E. O'Shea<sup>2</sup>, and J.G. Doyle<sup>1</sup>

<sup>1</sup> Armagh Observatory, College Hill, Armagh BT61 9DG, Northern Ireland

<sup>2</sup> Department of Pure and Applied Physics, The Queen's University of Belfast, Belfast, BT7 1NN, Northern Ireland  
(email: dipu@star.arm.ac.uk, E.Oshea@qub.ac.uk, jgd@star.arm.ac.uk)

Received 2 December 1999 / Accepted 13 January 2000

**Abstract.** We examine spectral time series of coronal line Mg IX 368 Å and transition region line O V 629 Å, observed with the Coronal Diagnostic Spectrometer (CDS) onboard the SOHO spacecraft. Primarily we were looking for intensity and velocity oscillations in polar plumes, however by chance we detected a giant macro-spicule at the limb and were able to follow its dynamical structure. Blue and red-shifted emission in the O V line indicates that it is probably a rotating twisted magnetic jet. Emission is also detected in the Mg IX 368 Å line, at a temperature of 1 million K.

Both Fourier and wavelet transforms have been applied independently to the analysis of the oscillations in order to find the most reliable periods. We report here on the existence of long period oscillations in the polar plumes as observed in the O V 629 Å line. Our observations indicate the presence of compressional waves with periods of 20–25 minutes.

**Key words:** waves – line: profiles – Sun: atmosphere – Sun: corona – Sun: oscillations – Sun: UV radiation

## 1. Introduction

Macro-spicules appear as columns of chromospheric material extending anywhere from 10 to 60 arcsec above the solar limb. Bohlin et al. (1975) first identified macro-spicules from Skylab spectrograph data in the He II 304 Å line. Their characteristic lifetimes range from 3 to 45 minutes (Dere et al. 1989). Moore et al. (1976, 1977) established that EUV macro-spicules could be associated with H $\alpha$  macro-spicules, which in turn seem to be related to flaring X-ray bright points. Chromospheric mass ejections in coronal holes has also been termed as giant macro-spicules (Loucif 1994). From the H $\alpha$  filtergrams taken from Sacramento Peak Observatory, Loucif (1994) has shown that they may significantly contribute to the fast solar wind. Examination of these structure shows that they are impulsive, recurrent and reach the corona. They seem to be located in the chromospheric network, and follow the assumed open magnetic field lines towards the solar corona. Usually the macro-spicules are

prominent in spectral lines formed around  $5 \cdot 10^4$  K but are invisible in lines formed above  $3 \cdot 10^5$  K. Previous EUV and radio observations suggest that macro-spicules have cool  $10^4$  K plasma cores, with a thin outer sheath not exceeding  $3 \cdot 10^5$  K (Withbroe et al. 1976; Habbal & Gonzalez 1991). We report here on the detection of a giant macro-spicule with O V 629 Å ( $2.5 \cdot 10^5$  K), and also with a high temperature coronal line, Mg IX 368 Å ( $1 \cdot 10^6$  K).

Previous observations by Hassler et al. (1997) and DeForest et al. (1997) did not find any obvious relationship between macro-spicules observed at the limb and polar plumes higher up, other than they both benefit from the open magnetic field configuration in the coronal hole. DeForest et al. (1997) have suggested (from EIT and MDI image overlays) that polar plumes seem to be related to, and originate from, small EUV bright points corresponding to quiescent, unipolar magnetic flux concentrations on network cell boundaries.

Pike & Harrison (1997) first reported the detection of a macro-spicule from a raster scan of CDS. They detected high velocity flows within the macro-spicule. Pike & Mason (1998) have further studied several macro-spicule-like dynamic events in polar regions and have indicated the presence of rotating plasma within the macro-spicule, which they named *solar tornados*. In contrast to earlier CDS raster scans, our temporal series allow us to study the dynamics of these events with better precision. Very recently, Parenti et al. (1999) have analysed a raster scan in the south polar coronal hole, including a macro-spicule and have presented information on density, temperatures and abundances.

Although spicules have been observed for many years, very little is known about their role in the transport of mass and energy between the chromosphere and higher layers of the Sun. The present investigation is concerned with an analysis of the temporal behaviour of the polar plume plasma. However during our temporal observations we also detected, quite by chance, a macro-spicule or small scale jet within the plume structure.

## 2. Observations and data reduction

The Coronal Diagnostic Spectrometer (CDS) onboard the Solar Heliospheric Observatory (SOHO) is a dual extreme ultraviolet spectrometer, covering the wavelength range 150 to 780 Å,

---

Send offprint requests to: D. Banerjee

\* current address: Center for Plasma Astrophysics, K.U. Leuven, 3001 Heverlee, Belgium

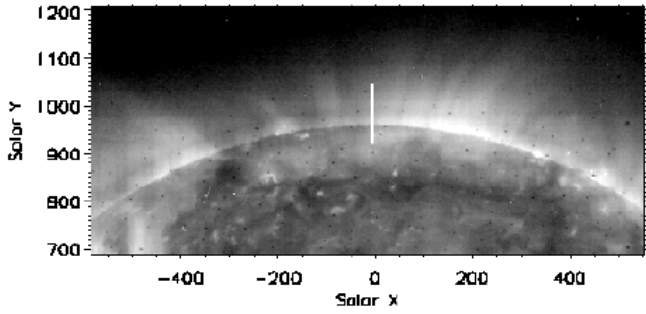


**Fig. 1.** Position of the observing slit for the s16834r00 dataset (15 July 1999) on an EIT images in Fe XII 195 Å (courtesy of the EIT consortium).

comprising of a normal incidence and a grazing incidence spectrometer (Harrison et al. 1995). The normal incidence spectrometer (NIS), whose data is the subject of this paper, gives spectral images in two wavebands (308–381 Å and 513–633 Å). In order to get good time resolution, we used the NIS in a sit-and-stare mode. For the data reported here, the  $4 \times 119$  arcsec slit was used. Although CDS has the ability to compensate for solar rotation, this was turned off since we did not want to introduce any possible variations due to instrument movements. These observations were obtained at a pointing of  $X=-6.5$ ,  $Y=+981$  and thus for these plume observations rotational compensation is not an important consideration. Fig. 1 shows an image of the north polar coronal hole region taken with EIT in Fe XII 195 Å at 22:12 UT on July 15, 1999 with the slit superimposed.

The data discussed here were obtained on the 15 July 1999 at 15:33 UT. The observations are summarised in Table 1. Two temporal series datasets were obtained for the three lines of O V 629 Å ( $\log T_e=5.4$  K), Mg IX ( $\log T_e=6.0$  K) and Fe XVI ( $\log T_e=6.3$  K). Data were obtained after the recovery of SOHO and so the lines show the characteristic broadened wings. This broadening has the effect of blending the Mg IX 368 Å line with that of the nearby Mg VII 367 Å line. Henceforth this blend will be referred to only as the dominant component of the blend, in this case Mg IX. To improve the signal-to-noise of this data we binned by three pixels along the slit, in effect creating new pixels of  $5 \times 4$  arcsec<sup>2</sup>. The data for the coronal line Fe XVI 335 Å were very weak and are therefore not included in the present analysis.

Using the standard CDS software procedure VDS-CALIB, we debiased and flat-fielded the data. The resulting data after running this procedure were in units of photon-events/pixel/sec. Multiplying by the exposure time yielded units of photon-events/pixel. In the result section counts means photon-events in the binned pixel. The data was cleaned of cosmic ray hits by using the CDS software procedure CDS.CLEAN.

Details of the Fourier analysis can be found in Doyle et al. (1999). Power spectra are obtained from the Fourier transforms of the auto-covariance functions, multiplied by a window function to reduce the variance of the noise. For the smoothed spectra we used the Tukey window. Power spectra are normalized in such a way that the expected mean noise level equals 2. Because the mean noise level and its variance are known we are

**Table 1.** Details of the temporal series observations

Date	15 July 1999
Observing sequence	CHROM_N4
	2 temporal series datasets: s16834r00, s16834r01
Pointing (X,Y)	-6.5, 983 (s16834r00) -6.5, 981 (s16834r01)
Starting time	15:33 UT (s16834r00) 17:27 UT (s16834r01)
Instrument	Coronal Diagnostic Spectrometer (CDS)/ Normal Incidence Spectrometer (NIS)
Region observed	North Polar Coronal Hole
Lines observed	O V 629 Å ( $\log T = 5.4$ K) Mg VII 367 Å/Mg IX 368 Å ( $\log T = 5.8/6.0$ K) Fe XVI 335 Å ( $\log T = 6.3$ K)
Slit size on Sun	$4 \times 119$ arcsec <sup>2</sup>
Binning along slit	3 pixels i.e. $3 \times 1.68$ arcsec (to produce new ‘pixels’ of $5 \times 4$ arcsec <sup>2</sup> )
Rotation compensation	Off
Cadence	30 sec

able to derive confidence limits for spectral features. For both intensity and velocity power spectra we use confidence levels of 99.9%. To determine the Doppler shifts, wavelength calibration is needed. We use the ‘limb method’, where we assume that above the limb all (non-radial) wave or mass motions on average cancel out. In the absence of radiative transfer effects, above limb Doppler shifts must on average be zero. This method was also used by Doschek et al. (1976) and Peter & Judge (1999). Note that Doppler shifts in the coronal hole are independent of the rest wavelength; everything is calibrated relative to the limb.

In order to find the most reliable periods, we have also performed wavelet analysis on the data. To this end we used the methods, techniques and software provided by Torrence & Compo (1998). This wavelet software uses the Morlet wavelet and moreover allows the calculation of confidence levels. Again we chose a confidence level of 99.9%. The benefits of using wavelet analysis is that the localised (in time) nature of the wavelet transform allows us to study the duration of any statistically significant oscillations as well as their period. For further details on wavelet analysis see Torrence & Compo (1998) and references therein.

### 3. Results

First we will discuss the results from the dataset s16834r00, during which we detected the macro-spicule. In Figs. 2 & 3, we show time slices of the observed O V 629 Å and Mg IX 368 Å respectively. In these plots, the solar north-south (SOLAR\_Y)

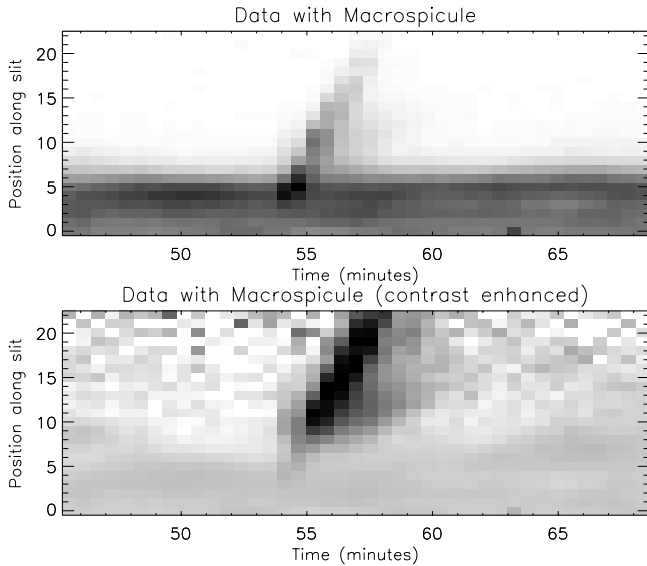


**Fig. 2.** The space-time behaviour of the intensity in the O v 629 Å line in the s16834r00 dataset. The gray scale coding has the most intense regions as dark. The lower image is contrast enhanced.

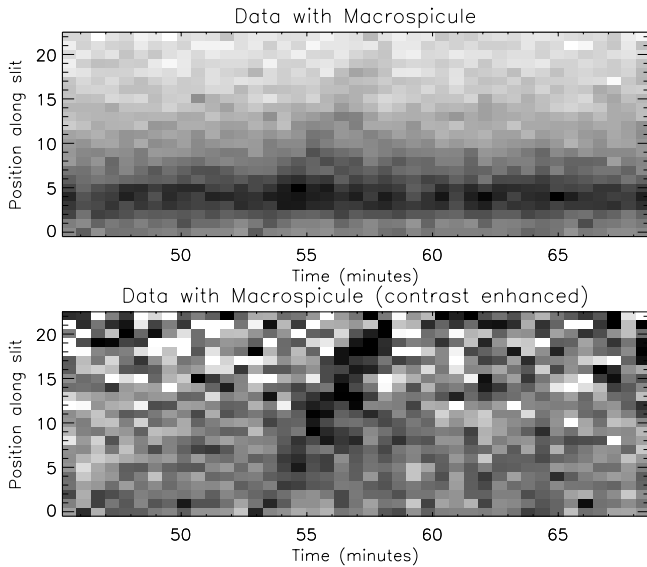


**Fig. 3.** Same as Fig. 2 for Mg IX 368 Å.

direction is in the vertical axis, the horizontal axis is time. To bring out details in the intensity map a contrast enhanced map is shown in the lower panels. This technique has been explained in detail in Doyle et al. (1999). Note that the macro-spicule event occurs between 53 to 58 minutes into the observing sequence. Although the Mg IX image (Fig. 3), is noisy due to low counting statistics, one can still see a bright jet like structure.

In Fig. 4, we show the temporal evolution map of the macrospicule intensity and velocity in O v. The contours are those of the O v intensities. Note that in the intensity map, the macrospicule shows extremely bright emission at its base. The brightest pixel in the velocity map shows a red shift of  $\sim 130 \text{ km s}^{-1}$ . The emission from the brightest region in the macro-spicule

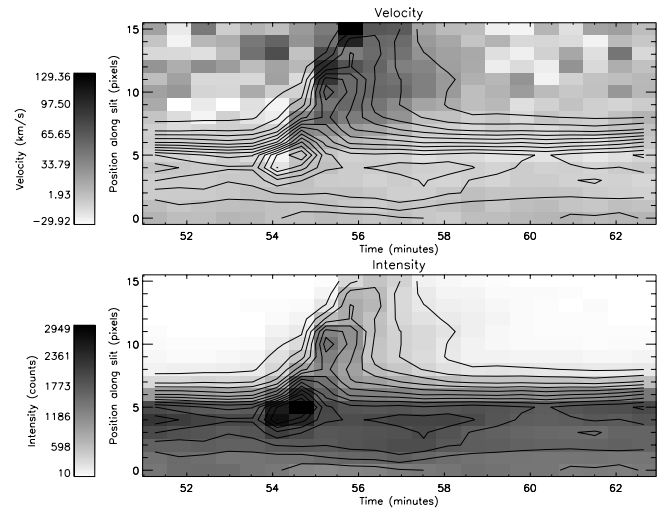


**Fig. 4.** Velocity and intensity temporal map for the event in s16834r00 as observed in O v 629 Å. The contour shows peak O v intensities.

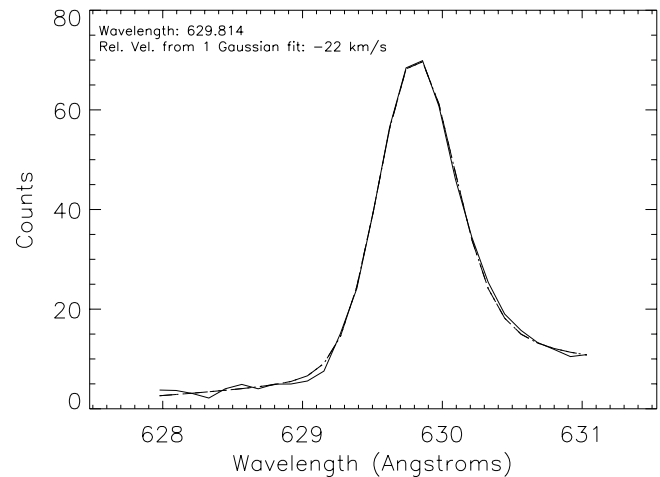


**Fig. 5.** For O v 629 Å line, a single broad Gaussian is fitted to the line corresponding to spatial pixel 8 and time 54 mins (see Fig. 4 for an overview of the location).

shows predominantly red shifted velocities, i.e., they are directed away from the observer. The left side shows much smaller velocities, and some positions on this side of the feature also show blue shifts, e.g. at positions 8-9 pixels and a time of 54 minutes. In Fig. 5 we show the line profile corresponding to pixel position 8 and time 54 minute, fitted with a Gaussian. It indicates a blue shift of  $22 \text{ km s}^{-1}$ . Note that at a later phase of the evolution of the macro-spicule, pixel position 11 and time 55.2 min, we find an average red shift of  $92 \text{ km s}^{-1}$  after fitting the line profile with a single Gaussian (see Fig. 6). Bear in mind that this is not a spatial map, rather a temporal map, thus it implies that in the initial phases of the macro-spicule we had strong blue-shifts, followed by red shifts in the decaying phase. This can be interpreted as a rotating feature - a sort of *solar tornado* as named by Pike & Mason (1998).

For a closer inspection of the intensity and velocity at individual locations in the SOLAR\_Y, we plot the data for a series

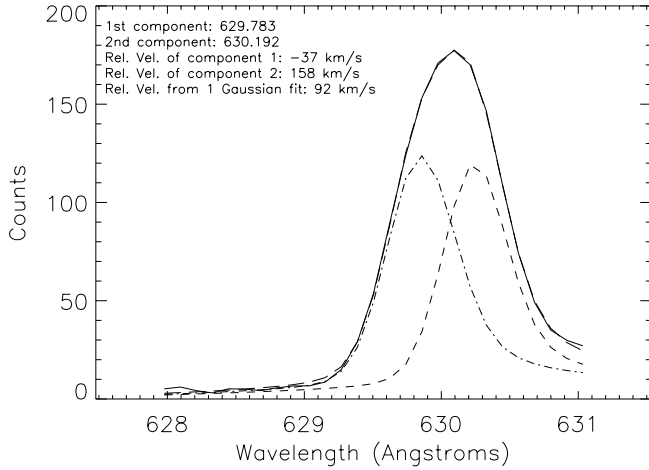


**Fig. 6.** For O v 629 Å line, a two component Gaussian is fitted to the data at spatial pixel 11 and time 55.2 mins (see Fig. 4 for an overview of the location).

of pixels in Fig. 7. This can also be viewed as horizontal slices of the ‘space-time’ plot and provides information about the radial dependence of intensity and velocity. The solid line represents the total counts and the dashed line represents the velocity. Note that pixel 4, which marks the limb, shows blue shifts during the event and as we progressively go outside the limb we have pronounced red shifts. This might indicate the presence of a double sided jet. Furthermore, the increase in Doppler velocities with height can be due to plasma accelerating outwards. There is clear evidence of acceleration of plasma from a distance of 20 to 45 arc sec above the limb (see 4th to 9th pixels). Above that altitude it tends to a constant apparent velocity. Thus a rotating accelerating plasma could explain the observation.

Now we turn our attention to the s16834r01 dataset, which was taken  $\sim 4$  seconds after the s16834r00 sequence and almost in the same location as s16834r00. The observation was programmed in such a way that the next sequence automatically traces back to the same location as the previous one. Therefore, within pointing errors we can assume that it is in the same part of the coronal plume plasma. Furthermore since we bin our data across 3 original pixels  $\sim 5$  arc sec, any difference in pointing should be minimum. In this part of the analysis we will study the oscillations in the plume plasma and also try to find out whether there is any effect of the macro-spicule on the plume oscillations.

A rotating plasma will also tend to asymmetrically broaden the line profiles. In order to examine this more closely, we attempted to fit two Gaussians to the profiles at several locations, particularly during the event when the single profile width was generally greater than the background. As an example of this we can look again at spatial pixel 11 at time 55.2 mins which is plotted in Fig. 6. At this location the observed line profile shows an asymmetric significantly broadened profile. If a single Gaussian is fitted the maximum red shift superficially corresponds to a redshift of around  $92 \text{ km s}^{-1}$  (as noted above). However, fitting with a two component Gaussian results in a blue shift of

$37 \text{ km s}^{-1}$  for one component and red shift of  $158 \text{ km s}^{-1}$  for the other, relative to the background.

### 3.1. Fourier transform

In the top left panel of Fig. 8, we show time slices of the observed O v 629 Å line in dataset s16834r01. Fluctuations in the bright features are clearly visible and their appearance seems periodic. These structures are so bright that in a gray scale presentation it is difficult to identify weakly emitting structures. To bring out details in the intensity map we use a technique based on enhancing the contrast of these structures, thereby filtering out the bright components in the brightness evolution displays (as done for the lower panels of Figs. 2 & 3).

The contrast enhanced space time behaviour is shown in the lower left panel. It clearly shows the periodic brightening of features with a periodicity of  $\sim 25$  minutes. The power spectra of the observed intensities at individual pixels along the slit, obtained from the Fourier transform are shown in the right lower panel of Fig. 8. The total number of counts in a pixel (summed counts) during the observation is shown in the upper right-hand panel, and is useful in identifying the solar limb and the plume. The O v power shows strong peaks between 0.2 to 1 mHz. From the overlay of EIT images and slit and also from the intensity variation across the slit we identify the 9th pixel (in our binned scale) to be just inside the plume structure. Thus we will now concentrate on this pixel and study its power spectra in greater detail.

In Fig. 10, the O v intensity and velocity power spectrum in a typical plume structure (9th pixel in the binned scale) is shown in panels (a) and (c) respectively. The lighter and the darker line correspond to the unsmoothed and smoothed power spectra respectively. The solid and dashed horizontal lines represent the 99.9% significance level of the unsmoothed power and the smoothed power respectively. The corresponding intensity and velocity variations with time are plotted in panels (b) and (d) respectively. The velocity oscillations are shown before (the lighter continuous line) and after a low-pass filter of everything above 4 mHz has been applied (the darker line). The O v intensity power shows a strong peak between 0.7 and 0.8 mHz, whereas the velocity power shows a peak at 1 mHz and a second peak around 0.6 mHz. Though on an average outside the limb the line shift should be zero, we do find the presence of a small blue shift (see Fig. 10d). We also find an anti-correlation between velocity and peak intensity as shown in Fig. 11. The ordinate have been normalized to arbitrary units for the overlay of intensity and velocity. Note that for the first 60 minutes of the observing sequence, when there is a peak in intensity the plasma is generally blue shifted (particularly when the oscillations are more prominent). Oscillation of long periods, are clearly visible in the light curves of Fig. 9. In this plot we show the light curves for the two consecutive time series s16834r00 and s16834r01. In principle these two light curves could be combined and one could then view it as a continuous time series of 227 minutes. The data drop out and the macro-spicule that occurred in dataset s16834r00 have been taken out and a linear interpolation applied

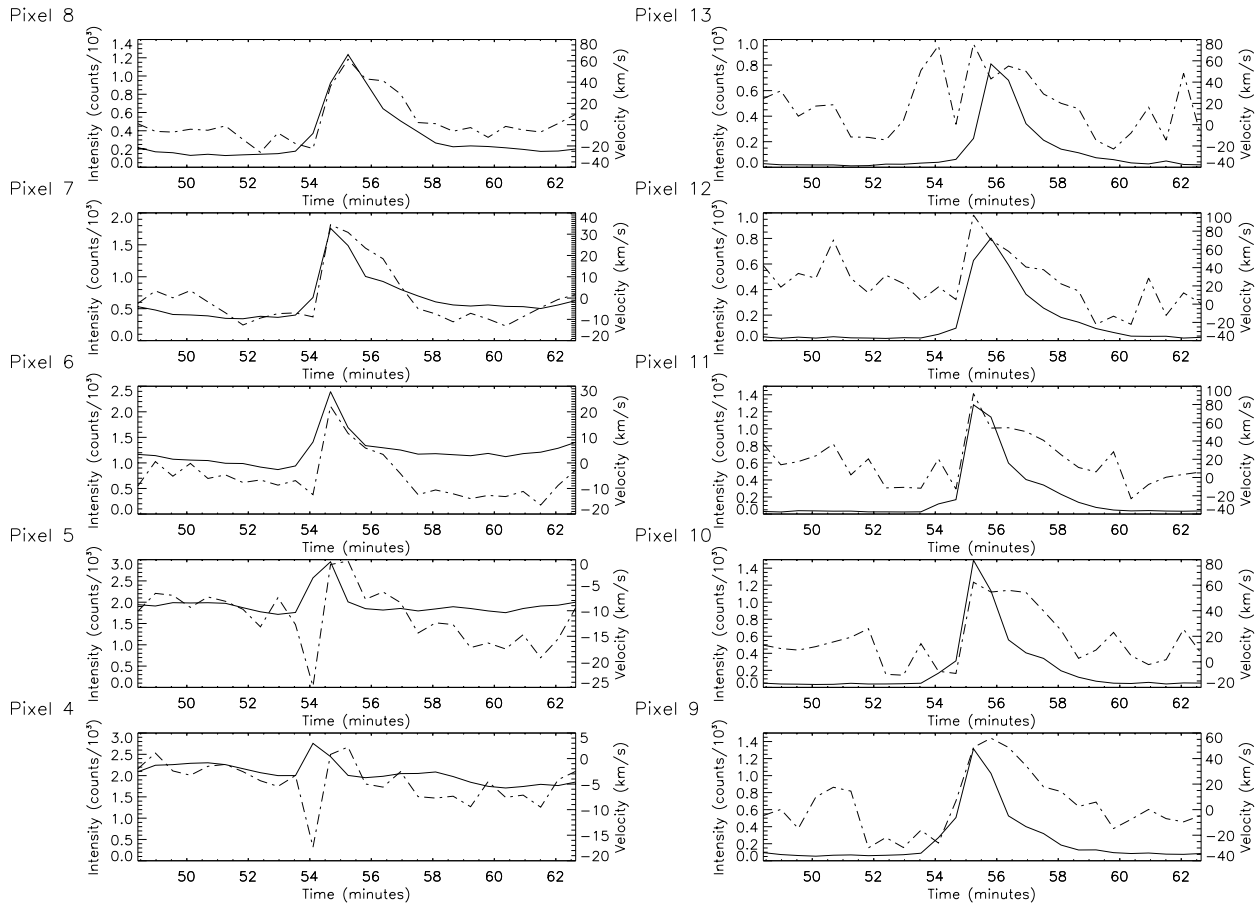


**Fig. 7.** The evolution of the macro-spicule event as observed in  $O\ v\ 629\ \text{\AA}$  intensity (solid line) and velocity (dashed line) at different SOLAR\_Y positions.

for those time intervals between 36.4–43.8 and 53.5–60.4 minutes. These interpolated regions are shown (plotted in Fig. 9) as the straight line sections between these times. The consecutive light-curves suggest that the macro-spicule has not affected the oscillations of the plume plasma. Furthermore the transit of the macro-spicule has not affected the periodicity of the plume plasma as it is still oscillating with a long period afterwards. This tends to indicate that although the macro-spicule has come across our field of view, while observing this particular north polar coronal plume, the macro-spicule is not connected with the plume structure.

### 3.2. Wavelet transform

The localised nature of time series analysis by wavelets makes them ideal for the data in s16834r00/r01. We should point out that wavelet transforms suffer from edge effects at both ends of the time series. The region in which these effects are important are defined by the ‘cone of influence’ (COI). The COI is an approximate measure that indicates the locations at which the results become unreliable due to these edge effects. We use the definition of COI given by Torrence & Compo (1998) but see also Meyers et al. (1993) for an alternate discussion.

In Figs. 12 & 13 we present the wavelet analysis for the intensity and the velocity respectively, corresponding to the sec-

ond time series s16834r01. The COI is marked as cross-hatched and any power over the 99.9% significance level is marked by continuous black line contours. On the right of these figures is plotted the global wavelet spectrum, which is just the average of the wavelet power spectrum over time. The dotted line in the global wavelet spectrum is again the 99.9% significance level. Torrence & Compo (1998) have pointed out that as the Fourier spectrum is smoothed, it approaches more and more closely the global wavelet spectrum. For the sake of comparison we present the results for the same 9th pixel as done previously for the Fourier analysis (see Fig. 10). The time frequency phase plot of the light-curve does indicate strong localised power between 0.7 mHz and 0.8 mHz during the major part of the time sequence. In comparison the velocity power is significant around 0.6 and 1 mHz. Note that the power is not significant during the last 20 minutes of the observing sequence, in either the intensity or the velocity.

## 4. Discussion

Suematsu et al. (1992) have suggested that spicules are generated by an impulsive upward force on the atmosphere such as shock wave propagating upwards and its seed perturbation might take place at a layer deeper than the chromosphere. We have studied here the effect of these giant macro-spicules or

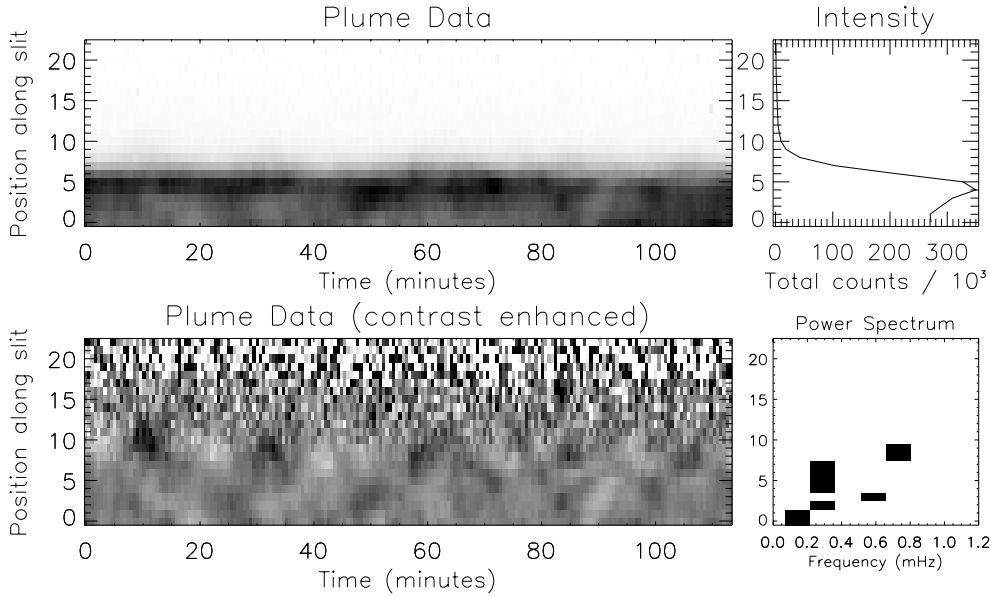


**Fig. 8.** The gray scale plots show the space-time behaviour of the intensity in the O v 629 Å line for the s16834r01 dataset. The gray scale coding has the most intense regions as dark. The upper right-hand panel show the counts summed over all time against the slit locations. The lower right-hand panel shows the power above the significance level as a function of frequency of oscillation and spatial position along the slit.

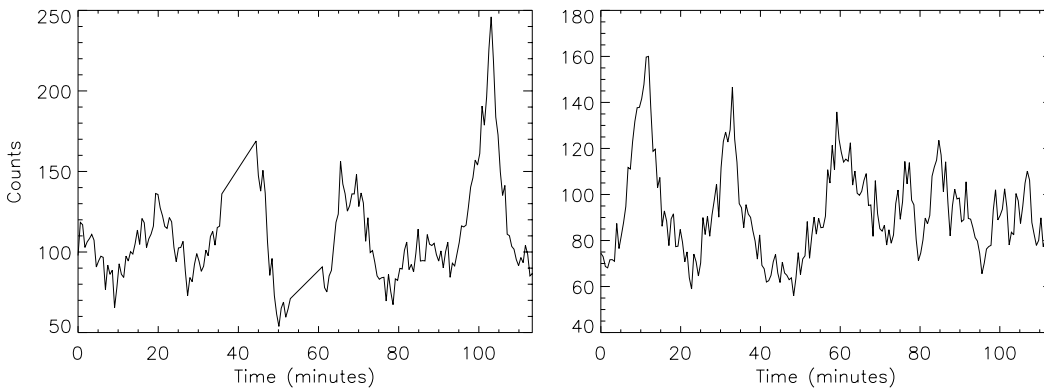


**Fig. 9.** The light curves corresponding to pixel position 9 in the two time series s16834r00 (left) and s16834r01(right). Note the clear presence of a long periodicity. In the left panel the data drop out and the macro-spicule has been taken out and the data linearly interpolated. These interpolated regions are plotted as the straight line sections between the times of 36.4–43.8 and 53.5–60.4 minutes.

small scale jets on the coronal plasma, particularly the plume conditions. In the first part we have studied the temporal evolution of the macro-spicule in our time series and in the second part, with various power spectra analysis techniques, studied the dynamics of the plumes.

Loucif (1994) have classified the existence of two classes of macro-spicules in the high chromosphere-transition zone: (a)- ‘classical’ macro-spicules, (b)- macro-spicules which evolve up to a critical height beyond which they eject a plasmoid. These plasmoids are impulsive, recurrent and reach the corona. Some of their velocities are supersonic; a succinct estimate of mass flux seems to confirm the in situ fast solar wind measurements realised by rocket flights.

Our observations suggest that we have encountered the ‘b’ type, the more dynamic macro-spicule type, in our temporal series. Following Pike & Mason (1998) we suggest that macro-spicules have a rotating as well as a jet-like structure. Over a considerable time interval we were able to show the continued existence of two velocity components, which further indicate that the plasma is rotating. Kudoh & Shibata (1997) have proposed a theoretical model for spicules which is based on the

concept of a rotating flux tube. They report MHD simulations of torsional Alfvén waves propagating through open magnetic flux tubes. They assume that the Alfvén waves are generated by random foot-point motions in the photosphere. Their model exhibits local enhancement of the O v emission. Our observed macro-spicule shows bright emission at its base. It has been detected not only in O v (250, 000 K) but also in Mg IX which is characteristic of a 1 million K plasma. We also find evidence of plasma acceleration between heights of 20–45 arc sec and then a plateau is reached. In the left side of the macro-spicule (see Fig. 4), we have found red-shifts of up to  $130 \text{ km s}^{-1}$ . We do not know the non-radial nature of the macro-spicule out of the plane of the image, so we can not calculate the actual velocities involved in the high speed solar wind. But if we assume that the macro-spicule is rooted this side of the limb and it is tilted from the plane of the sky, then a small velocity translates to a much larger actual wind speed. These properties of our observed macro-spicule match very well with those of Pike & Harrison (1997).

Our observations further indicate the presence of a double sided jet, namely blue shifts in the limb and red shifts outside

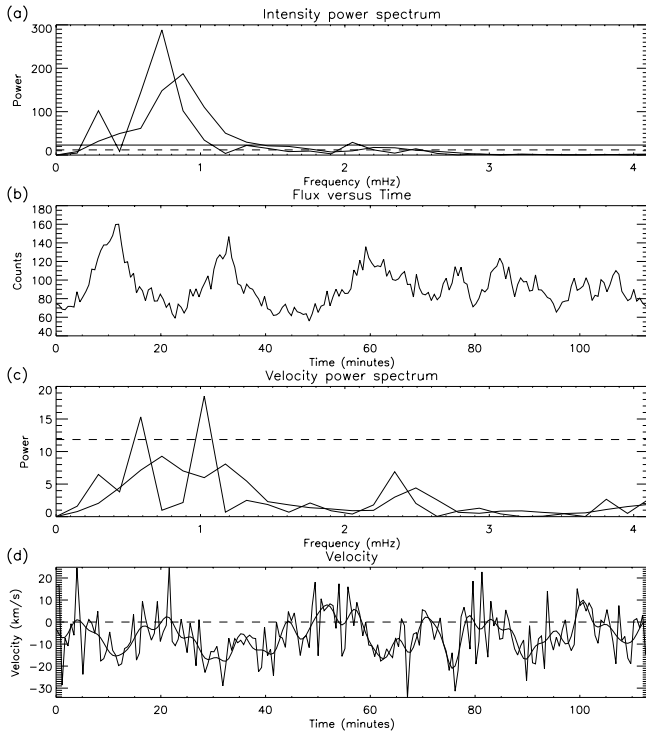


**Fig. 10a – d.** For pixel position 9 in the s16834r01 dataset & O v 629 Å line, **a** & **c** shows the intensity and velocity power spectra respectively. The lighter lines correspond to unsmoothed data and the darker lines correspond to the smoothed data. The solid and the dashed horizontal lines represent 99.9% significance levels for the unsmoothed and smoothed power respectively. Panel **b** shows the variation of intensity with time (light curve) while **d** shows the velocity oscillation. The velocity oscillations are shown before (the lighter continuous line) and after a low-pass filter of everything above 4 mHz has been applied (the darker line).

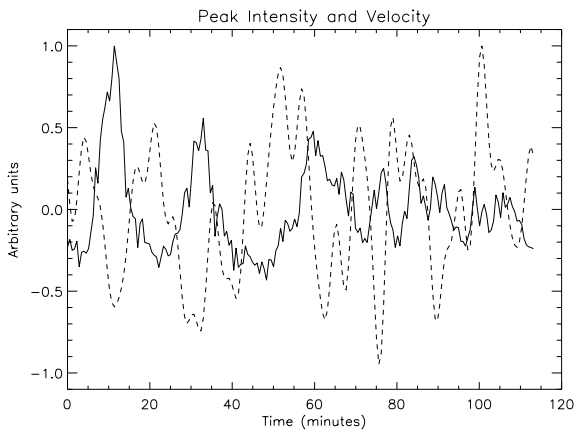


**Fig. 11.** For O v 629 Å line, the variation of intensity (solid line) and velocity (dashed line) with time corresponding to pixel position 9 of s16834r01 dataset.

the limb. A closer inspection of the space time plot (see the extreme right-side of the macro-spicule in Fig. 2) shows weak signatures of fragmentation or ballooning along the length of the macro-spicule. Habbal & Gonzalez (1991) from their radio data

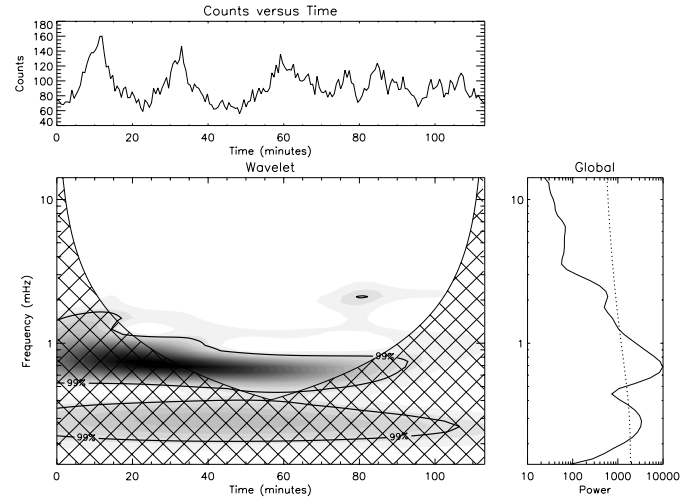


**Fig. 12.** The wavelet analysis for O v in the plume at the same location as in Fig. 10. The left panel shows the time frequency phase plane plot of the light-curve. The right panel shows the average of the wavelet power spectrum over time. The thick contour encloses regions of greater than 99.9% confidence. Cross-hatched regions, on either side indicate the ‘cone of influence’ where the edge effects become important. Note that maximum intensity power lies between 0.7-0.8 mHz (20-24 min periodicity).

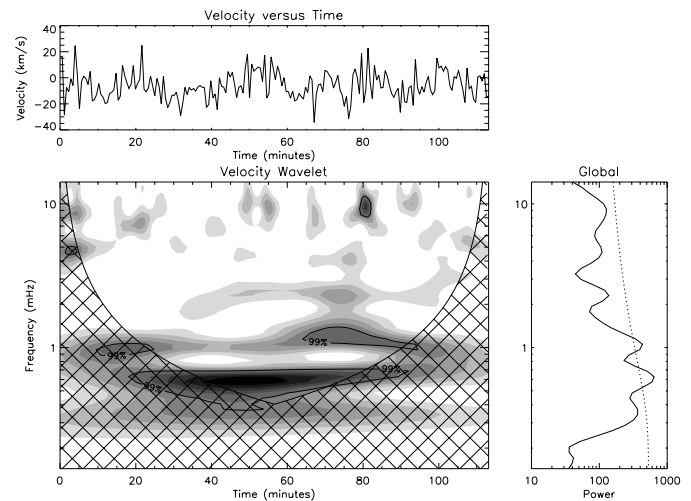


**Fig. 13.** Wavelet analysis for the O v 629 Å velocity, same as in Fig. 12. Maximum power lies around 0.65 mHz (25 min periodicity)

have found evidence of the pinching off or ballooning at higher altitudes in the macro-spicules. Our observations are quite consistent with the unified model proposed by Shibata (1997). In his simulation a twisted or sheared magnetic flux emerges to reconnect with the overlying field. He found that as a result of reconnection between twisted and untwisted fields, shear Alfvén waves are generated and propagate along magnetic reconnected field lines. Since these Alfvén waves have large amplitudes, they excite large transversal motions (or spinning motion) of jets and exert a nonlinear magnetic pressure force to cause further acceleration of the jet, as originally suggested by Shibata & Uchida (1986). Moore et al. (1977) proposed that macro-spicules are

associated with flaring bright points. It will be interesting to know whether macro-spicules are linked with bright points and X-ray jets. We hope that in the future co-ordinated observations with many instruments will be able to answer these questions.

High-cadence SOHO/EIT observations indicate that quasi-periodic fluctuations with periods 10–15 minutes are present in polar plumes (DeForest & Gurman 1998). They have also found that the fluctuations propagate outwards in the plumes at speeds 75–150 km s<sup>-1</sup>. Ofman et al. (1999) reported that the relative wave amplitude increases with height in the plumes out to about 1.2  $R_{\odot}$ . They believe that these are slow magneto-acoustic waves propagating through the plumes. Using the white light channel (WLC) of UVCS, Ofman et al. (1997) have also reported density fluctuations in coronal holes on a time scale of  $9.3 \pm 0.4$  minutes. This may indicate the presence of compressional waves farther out in the corona, at 1.9  $R_{\odot}$ .

Our observations do indicate the very clear presence of long period oscillations with periods of 20–25 minutes. The power spectra obtained by Fourier and wavelet transforms have each established the existence of these long periods. Even from the light curves (see Fig. 9), and also from the contrast enhanced space time plots (see middle panel of Fig. 8) one can clearly see a 25 minute period. We interpret the waves as slow magneto-acoustic in nature. Ofman et al. (1999) have presented an analytical solution for the propagation of the magneto-acoustic waves in a gravitationally stratified, linear, one-dimensional model of the polar plumes. They find that for typical coronal conditions, 10–15 minute waves are propagating in the plume. Waves with periods longer than 70 minutes will become evanescent. We feel that with a different set of parameters, their calculations can also give 25 minute periods.

Recently, Kudoh & Shibata (1999) have presented a magnetohydrodynamic simulation of torsional Alfvén waves propagating along an open magnetic flux tube in the solar atmosphere. They show that if the Alfvén waves are generated by random motions (with velocities greater than 1 km s<sup>-1</sup>) at the photosphere, the transition region is lifted more than  $\sim 5000$  km (i.e. a spicule is produced), the emission lines are broadened ( $\sim 20$  km s<sup>-1</sup>) and as the Alfvén waves propagate upwards they produce slow or fast waves through nonlinear coupling. Part of the Alfvén waves are reflected back in the transition region and the remaining waves propagate upwards to the corona. They contribute a significant energy flux of  $\sim 3.0 \cdot 10^5$  ergs s<sup>-1</sup> cm<sup>-2</sup> to heat the corona and also broaden the emission lines. Thus their simulation suggests that the non-thermal broadening, spicule formation and oscillations, all could be caused by Alfvén waves generated in the photosphere. This scenario is also consistent with our observations. Finally we remind the reader not to put too much emphasis on this one temporal sequence. We have

several temporal series in polar plumes observed with CDS, whose analysis is in progress. We hope to present these results in a subsequent paper.

*Acknowledgements.* Research at Armagh Observatory is grant-aided by the Department of Education for N. Ireland while partial support for software and hardware is provided by the STARLINK Project which is funded by the UK PPARC. Wavelet software was provided by C. Torrence and G. Compo, and is available at URL: <http://paos.colorado.edu/research/wavelets/>. This work was supported by PPARC grant GR/K43315, plus a short-term fellowship to DB from Armagh Observatory. We would like to thank the CDS and EIT teams at Goddard Space Flight Center for their help in obtaining the present data.

## References

- Bohlin, J.D., Vogel, S.N., Purcell, J.D., et al., 1975, ApJ 197, L133  
 DeForest, C.E., Hoeksema, J.T., Gurman, J.B., et al., 1997, Solar Phys. 175, 393  
 DeForest, C.E., Gurman, J.B., 1998, ApJ 501, L217  
 Dere, K.P., Bartoe, J.-D.F., Brueckner, G.E., Cook, J.W., Socker, D.J., Ewing, J.W., 1989, Solar Phys 119, 55  
 Doschek, G.A., Feldman, U., Bohlin, J.D., 1976, ApJ 205, L177  
 Doyle, J.G., van den Oord, G.H.J., O’Shea, E., et al., 1999, A&A 347, 335  
 Habbal, S.R., & Gonzalez, R.D., 1991, ApJ 376, L25  
 Harrison, R.A., Sawyer, E.C., Carter, M.K., et al. 1995, Solar Phys 162, 233  
 Hassler, D.M., Wilhelm K., Lemaire, P., et al., 1997, Solar Phys. 175, 375  
 Kudoh, T., & Shibata, K., 1997, Proc. of the Fifth SOHO workshop, ESA SP-404, 477  
 Kudoh, T., & Shibata, K., 1999, ApJ 514, 493  
 Loucif, M.L., 1994, A&A 281, 95  
 Meyers, S.D., Kelley, B.G., & O’Brien, J.J., 1993, Mon. Wea. rev. 121, 2858  
 Moore, R.L., Tang, F., Bohlin, J.D., Golub, L., 1976, Bull. Am. Astron. Soc. 8, 333  
 Moore, R.L., Tang, F., Bohlin, J.D., Golub, L., 1977, ApJ 218, 286  
 Ofman, L., Romali, M., Poletto, G., et al., 1997, ApJ 491, L111  
 Ofman, L., Nakariakov, V.M., & DeForest, C.E., 1999, ApJ 514, 441  
 Parenti, S., Del zanna, G., Bromage, B. J. I., 1999, Proceedings published in ESA SP Series (SP-448), ed. A. Wilson. 131  
 Pike, C.D., & Harrison, R.A., 1997, Solar Phys 175, 457  
 Pike, C.D., & Mason, H.E., 1998, Solar Phys 182, 333  
 Peter H., & Judge P. G., 1999, ApJ 522, L77  
 Shibata, K., 1997, Proc. of the Fifth SOHO workshop, ESA SP-404, 103  
 Shibata, K., & Uchida, Y., 1986, Solar Phys 103, 299  
 Suematsu, Y., Wang, H., Zirin, H., 1992, AAS 180, 07.02  
 Torrence, C., & Compo, G.P., 1998, Bull. Amer. Meteor. Soc. 79, 61  
 Withbroe, G.L., Jaffe, D.T., Foukal, P.V., et al. 1976, ApJ 203, 528